

Super-hard and superconducting boron clathrates in the prediction of U-B compounds

Juefei Wu¹, Dexi Shao², Junjie Wang³, Yu Han³, Bangshuai Zhu¹, Cuiying Pei¹, Qi Wang^{1,4}, Jian Sun^{3*} and Yanpeng Qi^{1,4,5*}

1. State Key Laboratory of Quantum Functional Materials, School of Physical Science and Technology, ShanghaiTech University, Shanghai 201210, China

2. School of Physics, Hangzhou Normal University, Hangzhou 311121, China

3. National Laboratory of Solid State Microstructures, School of Physics and Collaborative Innovation Center of Advanced Microstructures, Nanjing University, Nanjing 210093, China

4. ShanghaiTech Laboratory for Topological Physics, ShanghaiTech University, Shanghai 201210, China

5. Shanghai Key Laboratory of High-resolution Electron Microscopy, ShanghaiTech University, Shanghai 201210, China

* Correspondence should be addressed to Y.P.Q. (qiyp@shanghaitech.edu.cn) or J.S. (jiansun@nju.edu.cn).

Abstract

The binary metal borides provide a promising platform for searching unique materials with superconductivity and super-hardness under high pressure, owing to the distinctive bonding characters of boron. In this work, combined the first-principles calculations and crystal structure predictions, we predicted 4 exotic stoichiometries and 8 unique U-B compounds under high pressure. The predicted compounds have layered or caged structure units and 4 of them host high hardness under ambient pressure. By removal of the U atoms, we predicted three meta-stable boron clathrates at ambient pressure. Remarkably, the Vickers hardness of the predicted $C2/m$ -B₆ is estimated to be 49-53 GPa, and the $C2/m$ -B₁₂ is superconducting with the T_c value of 16.12 K. Our calculations enrich the phase diagram of binary metal borides and boron allotropes, providing insights for the future theoretical and experimental studies on unique materials.

Key words: uranium borides; boron allotropes; first-principles calculations; high pressure; superconductivity; hardness.

I. Introduction

Binary metal borides have a significant variety of morphologies including 3D polyhedron, 2D nets and 1D chains, stemming from the valence electrons of boron are insufficient to fill up the bonding states and tend to form covalent bonds with multi-centers [1-3]. The combination of the boron based structural units and different metal elements are fundamental to the fascinating properties of binary metal borides, including the superconductivity and mechanical properties [4], thus has gained tremendous research attention. For instance, the superconducting MgB_2 has a high transition temperature T_c of 39 K at ambient pressure, which ignites the investigations of exotic superconductors in borides [5, 6]. Recent study reports that $\alpha\text{-MoB}_2$ has the highest T_c in the transition metal borides with the value of 32.4 K at 109.7 GPa [7, 8]. Subsequently, the MgB_2 -like WB_2 becomes superconducting under high pressure with a T_c of ~ 17 K at 90 GPa [9, 10]. The Mo- d and W- d orbitals play crucial roles in the superconductivity of corresponding borides. In the theoretical aspect, CaB_2 is iso-structural to MgB_2 and hosts stronger electron-phonon coupling (EPC) with T_c of 48 K [11]. The predicted YB_6 composes of B_{24} units and is superconducting with a T_c of 12.78 K at ambient pressure [12]. Ref. 13 predicts LaB_8 consisting of B_{26} cages, which is thermodynamically stable above 70 GPa and the T_c increases to ~ 20 K at ambient pressure.

In addition to superconductivity, binary metal borides are promising for exploring super-hard materials (hardness ≥ 40 GPa) [14, 15] due to the strong covalent B-B bonds. The ReB_2 comprises boron layers and the hardness reaches 48 GPa in the experiment [16]. WB_4 contains hexagonal B layers and B dimers, proposed with the hardness of 43.3 GPa [17]. The stackings of FeB_{12} polyhedra columns construct FeB_4 , which leads to hardness of 62 GPa [18]. ZrB_{12} is made up of the B_{24} units with the hardness of 40 GPa [19]. Besides, theoretical works predict excellent hard and super-hard binary metal borides with diverse boron structure motifs. The predicted CrB_4 encompasses interconnected quadrilateral boron units with the hardness of 48 GPa [20]. WB_5 holds boron networks with the estimated hardness of 45 GPa [21]. The Ref. 22 predicts that ScB_3 contains ScB_{13} polyhedron and ScB_6 involves boron trigons, and their calculated hardness values are of 38.3 GPa and 39.8 GPa, respectively.

Meanwhile, the high hardness and superconductivity could coexist in binary metal borides as well. The predicted $\alpha\text{-BeB}_6$ is a super-hard material (46 GPa) with T_c of 9 K, and the high pressure phase $\beta\text{-BeB}_6$ has hardness of 31 GPa and T_c of 21 K [23]. Ref. 24 predicts a class of hard superconductors constituted of B_{23} cages, such as

KB₇ (hardness 22.5 GPa and T_c 26.2 K) and SrB₇ (hardness 25.1 GPa and T_c 12.67 K). Ref. 25 proposes the hardness values of clathrate structures LiB₄ and NaB₄ are about 39 GPa, and their T_c values are of 6 K and 8 K, respectively. Recent study on clathrate-like CeB_n compounds report the hardness of 20-39 GPa, and T_c values are of 29 K and 27 K for CeB₂ for CeB₈, respectively [26].

Moreover, binary metal borides can act as precursors to achieve boron allotropes with high hardness and superconductivity. The clathrate NaB₄ and Na₂B₁₇ are the precursors of B₄ (T_c 19.8 K) and B₁₇ (T_c 15.4 K), respectively [27]. Ref. 28 enhances the T_c record in elemental superconductors and predicts caged *t*-B with the T_c value of 43 K at ambient pressure, which is much higher than its precursor *t*-MnB₁₂ ($T_c \sim 7$ K) formed by B₁₆ cages. The predicted *o*-B₁₆ exhibits T_c of 14.2 K and hardness of 19.4 GPa, which originates from the removal of Sr atoms in the SrB₈ featuring anticlinal pentapyramids units [29].

Therefore, the above results suggest that both the unique boron morphologies and appropriate metal elements are key factors for pursuing either super-hard materials or superconductors in binary metal borides, which may also benefit for searching exotic boron allotropes with interesting properties. Inspiring by the researches of superconducting hydrides under high pressure, the element uranium could help to reduce the stable pressure and play crucial role in the electronic structures and EPC of hydrides [30-34]. Besides, the stoichiometries along with the layered or caged structure units of the known U-B compounds UB₂, UB₄ and UB₁₂ [35, 36] illustrate the potential to predict unique boron-rich structures under high pressure. In addition, UB₂ is also a potential candidate as safer fuel for Generation IV nuclear reactors [35], while the studies of U-B compounds under high pressure are relatively limited. Thus, it is intriguing to study the U-B compounds under high pressure. In this work, we explore the U-B compounds by combining the first-principles calculations and the machine learning graph theory accelerated crystal structure search method within 200 GPa. We predict 4 exotic stoichiometries and 8 unique U-B compounds, and 4 of them have high hardness under ambient pressure. By removing the uranium atoms, we predict 3 boron clathrates with meta-stability at ambient pressure. Among them, the Vickers hardness of the predicted *C2/m*-B₆ is estimated to be 49-53 GPa, and *C2/m*-B₁₂ is superconducting with the T_c value of 16.12 K.

II. Methods

Firstly, we conducted first-principles calculations to evaluate the influence of the on-site Coulomb repulsion effects on the localized $5f$ electrons of U atoms in U-B compounds based on the experimental data under high pressure [35]. We used the Vienna *Ab-initio* Simulation Package (VASP) based on the density functional theory [37, 38], and the detailed settings are listed in Supplementary file [39]. The test results are shown in Table. S1 [39], the Coulomb repulsion has negligible impact on the lattice parameters, and the results match well with the experiment data without Coulomb repulsion under high pressure [39]. This is analogous to the small effect of Coulomb repulsion in U-H compounds under high pressure [31, 32].

Then we carried out the crystal structure searches by combining VASP with the machine learning and graph theory assisted universal structure searcher (MAGUS) [43, 44], conducting variable composition structure searches to construct the convex hulls. Fixed composition structure searches were further performed for each stable stoichiometry to validate the results. The exchange-correlation functional was the generalized gradient approximation (GGA) of Perdew, Burkey, and Ernzerhof [45], and valence electrons of $5f^2 6s^2 6p^6 6d^2 7s^2$ in U and $2s^2 2p^1$ in B are treated by the projector-augmented wave (PAW) approach [46] for geometry optimization and electronic structure calculations. To study the chemical bonding properties, we performed the crystal orbital Hamilton population (COHP) analysis using the LOBSTER 4.1 package with the pbeVasFit2015 basis set [47]. The phonon spectra were calculated by the PHONOPY program package [48]. To further access the thermal stability, we conducted *ab initio* molecular dynamics (AIMD) simulations under NVT ensemble (N , V , and T are the number of particles, volume, and temperature, respectively) through the Nosé-Hoover approach [49], which is rechecked by NPT ensemble (P is pressure) as well. The elastic constants were calculated using the strain-stress method [50], and we employed the Voigt-Reuss-Hill approximation to derive the bulk modulus B (GPa), shear modulus G (GPa) and Young's modulus E (GPa) [51]. The Vickers hardness (H_v) is estimated by Chen's formula (H_v^{Chen}) [52], Tian's formula (H_v^{Tian}) [53] and Mazhnik's formula ($H_v^{Mazhnik}$) [54]. The electron-phonon coupling (EPC) constants were calculated by the QUANTUM-ESPRESSO (QE) package [55]. More detailed parameters for the above calculations can be seen in the Supplementary material [39].

III. Results and discussion

A. Structures and stability of U-B compounds

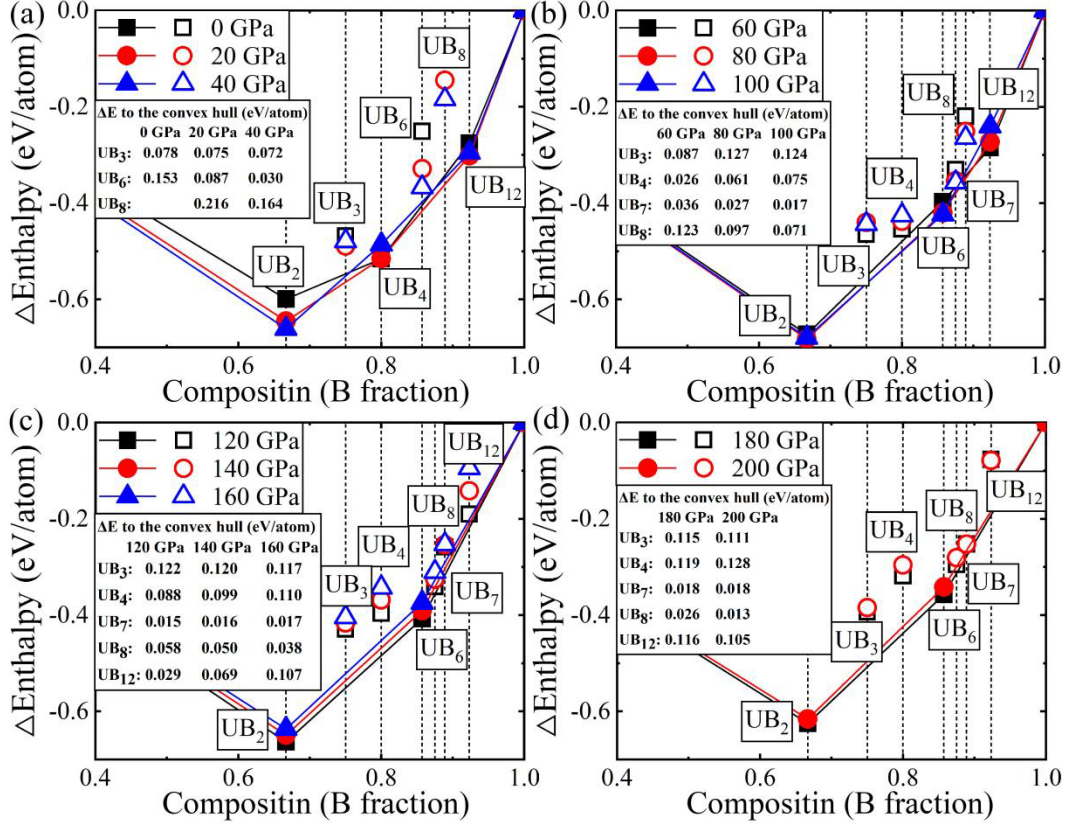


FIG. 1. The convex hull diagrams for U-B compounds under high pressure. The solid points indicate that the stoichiometries are on the convex hull, while the empty points are above the convex hull.

In this work, we explore the stable phases of U-B compounds under high pressure and conducted structure searches at 50, 100, 150 and 200 GPa, respectively. We recalculate the enthalpies of the predicted structures to construct the convex hull with the simple substances U and B [56-58] as the references under high pressure. As shown in Fig. 1, we predicted 4 unique stoichiometries UB₃, UB₆, UB₇ and UB₈. Since all the stoichiometries are on the boron-rich side, the convex hull starts from the B/(U+B)=0.5 site. In Fig. 1 (a), the known stoichiometries UB₂, UB₄ and UB₁₂ lie on the convex hull at 0 GPa, the consistency with the experimental results [35] suggest the feasibility of our calculation methods. UB₂ remains on the convex hull up to 200 GPa, while UB₄ falls off the convex hull after 60 GPa and the enthalpy difference relative to the convex hull increases with the pressure. Simultaneously, the predicted stoichiometry UB₆ emerges after 60 GPa and persists within the calculated pressure range. With further compression, the known stoichiometry UB₁₂ has analogous trend with UB₄, which leaves the convex hull since 120 GPa. Besides, the predicted stoichiometries UB₃, UB₇ and UB₈ approach the convex hull with pressure increasing,

in particular UB₈ after 120 GPa.

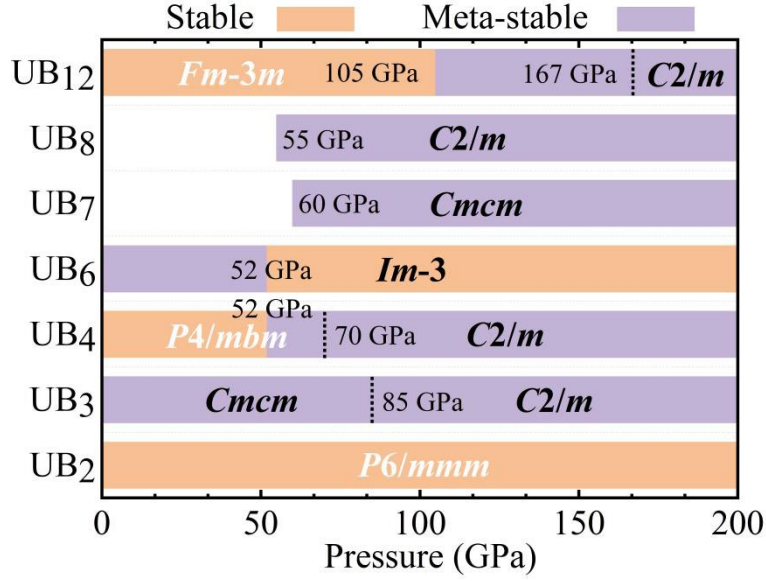


FIG. 2. The pressure-composition phase diagram of the U-B compounds. The predicted structures are in black bold font, while the reported structures are in white font. The orange region is the stable state and the violet region is the meta-stable state. The dashed lines suggest the phase transition pressure in the stoichiometry.

Then we calculated the detailed relative enthalpies [Fig. S1] [39] and the phonon spectra [Fig. S2-S3] [39] for the phase diagram of U-B compounds under pressure [Fig. 2]. To distinguish the thermodynamic meta-stability, a common threshold is of 50 meV/atom in the field of structures predictions [59], while the threshold of 200 meV/atom is employed for predictions in regard to the synthesized metal compounds [60]. Besides, the relative formation energy could reach 300 meV/atom in HfB [61], and the meta-stable Al_{1.28}B phase has positive formation energy around 208 meV/atom [62]. Hence we take the relatively intermediate threshold of 130 meV/atom for the meta-stability border anchoring the Mn-B compounds under high pressure [28]. The structure searches predicted 8 structures including UB₃-*Cmcm*, UB₃-*C2/m*, UB₄-*C2/m*, UB₆-*Im-3*, UB₆-*Cmcm*, UB₇-*Cmcm*, UB₈-*C2/m* and UB₁₂-*C2/m*, all of which have potential for synthesizing under high pressure. The calculated lattice parameters of the predicted structures are listed in Table. S2 [39]. The phonon spectra of the predicted structures have no imaginary frequencies [Fig. S2-S3] [39], indicating their dynamical stability within the corresponding pressure ranges. In addition, we calculated the zero point energy (ZPE) and estimated the temperature effect on the convex hull diagrams [Fig. S4] [39]. In Fig. S4 (a) and (d) [39], the enthalpy difference relative to the convex hull have slight changes, while the nodes of the convex hull and the thermodynamic stability keep consistent. Besides, the temperature

effect has less effect on the convex hull diagrams [Fig. S4 (b) and (d)] [39]. Hence we believe that the effect of ZPE could be negligible. According to our calculations, both UB_3 - $Cmcm$ and UB_3 - $C2/m$ are thermodynamically meta-stable under high pressure [Fig. S1(a)] [39] and they are dynamically stable at ambient pressure [Fig. S2(a)-(d)] [39]. Because of the emergence of UB_6 , the known structure UB_4 - $P4/mbm$ becomes meta-stable after 52 GPa and we predict a structural transition to UB_4 - $C2/m$ about 70 GPa [Fig. S1(b)] [39]. As plotted in the inset of Fig. S1 (c) [39], the predicted UB_6 - $Im-3$ is accompanied with a meta-stable structure UB_6 - $Cmcm$. Meanwhile, UB_6 also breaks the thermodynamic stability of UB_7 and UB_8 , keeping them from the convex hull under high pressure [Fig. S1 (d) and (e)] [39]. As for UB_{12} [Fig. S1(f)] [39], the known structure UB_{12} - $Fm-3m$ enters the meta-stable state since 105 GPa and it transforms to the predicted UB_{12} - $C2/m$ around 167 GPa. UB_{12} - $C2/m$ is not dynamically stable at the ambient pressure, but becomes stable until the critical pressure of 40 GPa [Fig. S3(g)] [39].

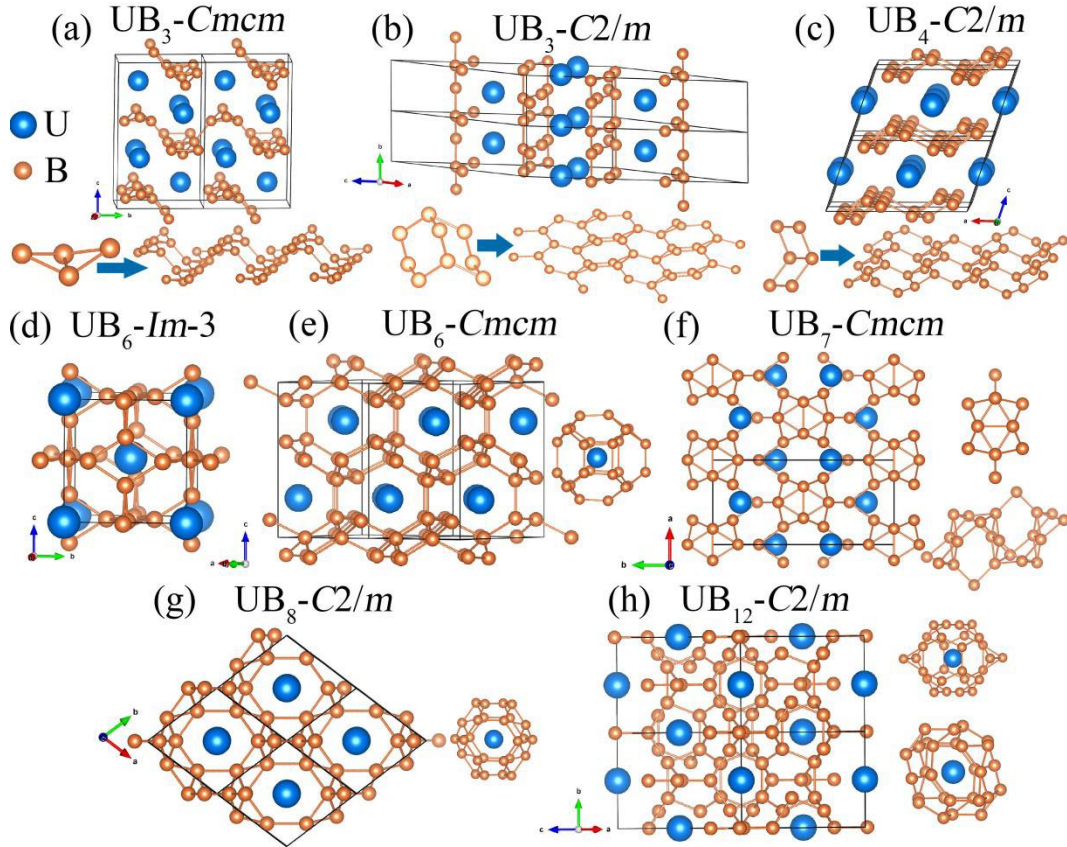


FIG. 3. The crystal structures of the predicted U-B compounds. The insets are the structure units.

As shown in Fig. 3 (a)-(c), the crystal structures of the predicted UB_3 - $Cmcm$, UB_3 - $C2/m$ and UB_4 - $C2/m$ are constructed by the stacking of boron networks with the uranium atoms embedded between the networks. The basic unit in the predicted UB_3 - $Cmcm$ is the two-fold boron triangles [inset of Fig. 3(a)]. The units form the

boron chains and the connection between the chains result in the waved boron layer in $\text{UB}_3\text{-Cmcm}$. The boron nets in the predicted $\text{UB}_3\text{-C2/m}$ are composed of a two-fold six-member rings [inset of Fig. 3(b)], while the nets in the predicted $\text{UB}_4\text{-C2/m}$ is composed of the four-member rings [inset of Fig. 3(c)]. We can observe flat hexagons between the structure units in both $\text{UB}_3\text{-C2/m}$ and $\text{UB}_4\text{-C2/m}$. In Fig. 3 (d), the four-member and six-member rings of boron atoms construct a B_{24} cage in the cubic $\text{UB}_6\text{-Im-3}$, resembling the hydrogen cages in the hydrides under high pressure [34]. Since the basic unit of $\text{UB}_6\text{-Cmcm}$ [Fig. 3(e)] is the distorted B_{24} cages of $\text{UB}_6\text{-Im-3}$, we can regard $\text{UB}_6\text{-Cmcm}$ as the sliding of the $\text{UB}_6\text{-Im-3}$. In terms of the predicted $\text{UB}_7\text{-Cmcm}$ [Fig. 3(f)], the boron atoms arrange in columns, with the uranium atoms embedding between boron columns. Both $\text{UB}_8\text{-C2/m}$ and $\text{UB}_{12}\text{-C2/m}$ exhibit clathrate features, in which the boron cages form channels and encircle the guest uranium atoms. The boron cages in $\text{UB}_8\text{-C2/m}$ and $\text{UB}_{12}\text{-C2/m}$ contain relatively distorted rings. The B_{26} cage in the $\text{UB}_8\text{-C2/m}$ [Fig. 3(g)] consists of four-member, twisted five-member and six-member rings, while the B_{28} cage in the $\text{UB}_{12}\text{-C2/m}$ [Fig. 3(g)] is composed of five-member and twisted six-member rings.

B. Electronic structures and mechanical properties

We calculated the band structures and projected density of states (PDOS) of the predicted U-B compounds at their corresponding lowest dynamically stable pressure, as illustrated in Fig. S5 and S6 [39]. The valence bands and conduction bands overlap with each other around the Fermi energy in all the predicted U-B compounds, indicating typical metal features. Despite the contribution of B atoms to the PDOS around the Fermi energy enhances with the B content, such as in $\text{UB}_7\text{-Cmcm}$ and $\text{UB}_{12}\text{-C2/m}$, the U-*f* electrons play dominant role in the PDOS around the Fermi energy in all the predicted U-B compounds. By calculating the electron localization function (ELF), we analysed the bonding types in B-B and U-B in the predicted U-B compounds. As shown in Fig. S7 [39], the bonds between B atoms indicates covalent interactions in the nets and cages. Nevertheless, we can find the connections between U atoms and B atoms, suggesting the U-B bonds are more covalent than ionic. It is similar with the interactions in binary U-H [30-32] and ternary U-Ca-H [34], in which the U-*f* electrons give rise to the metallicity in these hydrides. To further understand the bonding properties of the predicted U-B compounds, we performed the COHP and integrated COHP (ICOHP) calculations. According to the convention, the positive and negative values of -COHP represent bonding and anti-bonding characteristics and ICOHP could identify the bonding strength. As plotted in Fig. S8 [39], both bonds

between B-B and U-B are overall localized in the positive region of -COHP below the Fermi energy, illustrating the bonding fingerprints of B-B and U-B in all the predicted U-B compounds. The ICOHP results are listed in Table. 1, the bond strength of B-B is not only stronger than U-B in U-B compounds, but also stronger than the B-B bonds proposed in NaB₄ [25], MnB₁₂ [28], SrB₈ [29] and is comparable to the boron allotrope *o*-B₁₆ [29]. Furthermore, the ICOHP absolute value of U-B bonds is larger than that of Na-B, Mn-B and Sr-B [25, 28, 29], which accords with the ELF feature in Fig. S7 [39]. The stronger bond strength implies the potential of high hardness in the predicted U-B compounds. Besides, The Mulliken charge analysis demonstrate that the U atoms at most transfer 1.50 e⁻/atom to B atoms in UB₆-*Im*-3 and UB₆-*Cmcm*, and we find that the bond distances have almost negative correlation with the bond strength in U-B. Moreover, we also calculated the EPC properties of the predicted U-B compounds, only UB₆-*Cmcm* and UB₈-*C2/m* are possible superconductors with the EPC constants λ 0.30 and 0.35, suggesting weak superconductivity with estimated T_c values < 1 K.

TABLE. 1. The averaged ICOHP, averaged bond length and charge transfers of the predicted U-B compounds.

	Pressure (GPa)	B-B ICOHP (eV/pair)	U-B ICOHP (eV/pair)	B-B bond (Å)	U-B bond (Å)	B charge (e ⁻ /atom)	U charge (e ⁻ /atom)
UB ₃ - <i>Cmcm</i>	0	-5.58	-1.65	1.77	2.73	-0.27	0.82
UB ₃ - <i>C2/m</i>	0	-5.40	-1.95	1.78	2.70	-0.33	1.01
UB ₄ - <i>C2/m</i>	0	-5.79	-1.89	1.74	2.69	-0.28	1.13
UB ₆ - <i>Im</i> -3	0	-5.53	-1.55	1.76	2.74	-0.25	1.50
UB ₆ - <i>Cmcm</i>	0	-5.79	-1.52	1.75	2.74	-0.25	1.50
UB ₇ - <i>Cmcm</i>	60	-5.53	-2.47	1.70	2.52	-0.14	0.97
UB ₈ - <i>C2/m</i>	20	-5.55	-2.41	1.74	2.57	-0.17	1.36
UB ₁₂ - <i>C2/m</i>	40	-5.62	-1.65	1.70	2.70	-0.12	1.40

Furthermore, we calculated the mechanical properties of the predicted U-B compounds including bulk modulus B (GPa), shear modulus G (GPa), Young's modulus E (GPa) and Vickers hardness (H_v) using different formulas. The predicted U-B structures satisfy mechanical stability on the basis of Born stability criteria [63]. As listed in Table. 2, the hardness of UB₃-*Cmcm*, UB₃-*C2/m*, UB₄-*C2/m* and UB₆-*Im*-3 exceed 20 GPa at ambient pressure, in particular UB₃-*Cmcm* (29.59 GPa)

and $\text{UB}_3\text{-C2}/m$ (27.39 GPa). The hardness are comparable to NaB_4 [64], KB_7 , SrB_7 [24] and CeB_n [26], illustrating the predicted U-B compounds are potential high hardness materials.

TABLE. 2. The bulk modulus B (GPa), shear modulus G (GPa), Young's modulus E (GPa) and the Vickers hardness (H_v) estimated by different formulas [52-53] of the predicted U-B compounds.

	Pressure (GPa)	B (GPa)	G (GPa)	E (GPa)	σ	H_v^{Chen} (GPa)	H_v^{Tian} (GPa)	H_v^{Mazhnik} (GPa)
$\text{UB}_3\text{-Cmcm}$	0	218.60	177.98	419.97	0.18	29.59	28.55	25.75
$\text{UB}_3\text{-C2}/m$	0	215.87	169.62	403.24	0.19	27.39	26.50	23.20
$\text{UB}_4\text{-C2}/m$	0	218.13	164.43	394.23	0.20	25.43	24.74	21.09
$\text{UB}_6\text{-Im-3}$	0	245.38	169.18	412.69	0.22	23.04	22.80	19.62
$\text{UB}_6\text{-Cmcm}$	0	235.66	150.68	372.62	0.24	19.28	19.27	17.14
$\text{UB}_7\text{-Cmcm}$	60	453.27	306.82	751.00	0.22	33.11	34.03	35.22
$\text{UB}_8\text{-C2}/m$	20	286.20	160.94	406.61	0.26	16.93	17.45	19.41
$\text{UB}_{12}\text{-C2}/m$	40	328.55	231.18	561.78	0.22	29.01	29.10	27.25

C. Boron clathrates

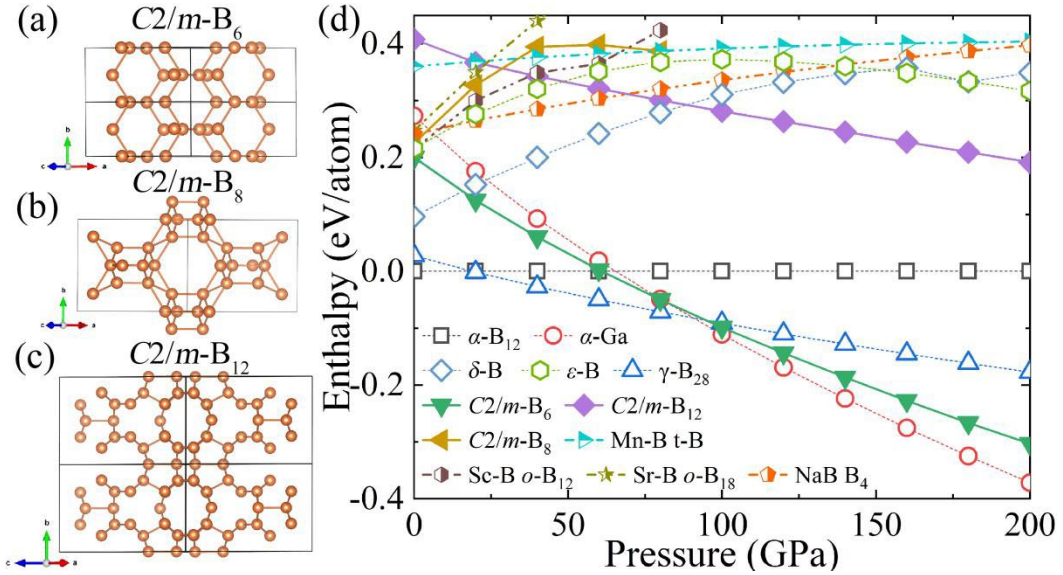


FIG. 4. (a)-(c) The crystal structures of the predicted boron clathrates at ambient pressure. (d) The enthalpy difference of the boron allotropes relative to $\alpha\text{-B}_{12}$. The t-B, $o\text{-B}_{12}$, $o\text{-B}_{18}$ and B_4 are predicted structures in Ref. 22, 27-29, $\delta\text{-B}$ and $\varepsilon\text{-B}$ are experimentally synthesized meta-stable boron allotropes in Ref. 65.

Since the predicted U-B compounds are made up of the boron networks or cages,

they may act as precursors for unique boron allotropes. By removing the U atoms in the predicted U-B compounds, we optimized the boron structures and calculated their phonon spectra under different pressures. 4 boron clathrate structures are dynamically stable at ambient pressure, including $C2/m$ -B₆ from UB₃- $C2/m$, $I4/mmm$ -B₄ from UB₄- $C2/m$, $C2/m$ -B₈ from UB₈- $C2/m$ and $C2/m$ -B₁₂ from UB₁₂- $C2/m$. Among them, $I4/mmm$ -B₄ has been reported with a T_c of 19.8 K at ambient pressure [27]. As depicted in Fig. S9 [39], the predicted boron clathrates $C2/m$ -B₆ and $C2/m$ -B₁₂ can host their dynamic stability until 200 GPa, while the structure of $C2/m$ -B₈ collapses after 60 GPa. The crystal structures of $C2/m$ -B₆, $C2/m$ -B₈ and $C2/m$ -B₁₂ are in Fig. 4 (a)-(c), the boron layers in Fig. 3(b) bond with each other after the removal of the U atoms, which lead to the clathrate structures of $C2/m$ -B₆. The predicted $C2/m$ -B₈ and $C2/m$ -B₁₂ retain the boron structure characters of their corresponding compounds [Fig. 3 (g) and (h)]. We calculated the enthalpy differences of $C2/m$ -B₆, $C2/m$ -B₈, $C2/m$ -B₁₂ and the boron allotropes reported by experiments and theoretical predictions [22, 27-29, 54, 55, 62] relative to the known α -B₁₂ under high pressures. As shown in Fig. 4 (d), although the enthalpy indicates that $C2/m$ -B₆ is meta-stable when comparing with the α -B₁₂ at ambient pressure, $C2/m$ -B₆ has lower enthalpy value than the synthesized meta-stable boron allotrope of ε -B at 0 GPa and δ -B at 20 GPa, respectively [65]. With further compression, the enthalpy value of $C2/m$ -B₆ is lower than the reported α -B₁₂ after 60 GPa and γ -B₂₈ around 90 GPa, which indicates the synthesizing potential. Besides, the enthalpy of $C2/m$ -B₈ is around 0.010 eV/atom above the synthesized ε -B at 0 GPa, and the enthalpy of $C2/m$ -B₁₂ approaches that of ε -B with increasing pressure, which is lower than that of ε -B after 50 GPa. In the aspect of synthesizing, we propose that one possible route is the combination of precursors and thermal degassing under dynamical vacuum, such as the synthesis of Si-24 from Na₄Si₂₄ [66], the other route is analogous to the meta-stable boron allotropes of both δ -B and ε -B. They are synthesized from β -B with the region of pressures 7.5-18 GPa and temperatures of 1373-2373 K [65] using diamond anvil cell (DAC) and laser heating. This suggests that appropriate choice of raw materials and pressure-temperature (P-T) condition are key factors for meta-stable boron allotropes. Considering the relative enthalpy value of the synthesized boron allotropes and other predicted boron structures (t-B, o -B₁₂, o -B₁₈ and B₄) [22, 27-29] in Fig. 4(c), we assume that δ -B with pressure range of 10-20 GPa, ε -B around 0 GPa and ε -B around 50 GPa could be suitable for $C2/m$ -B₆, $C2/m$ -B₈ and $C2/m$ -B₁₂, respectively.

Then we calculated the electronic structures of the predicted boron clathrates. The

ELF of the predicted boron clathrates are shown in Fig. S10 [39], the boron atoms have strong covalent interactions and the empty region reflect the channels of the clathrate structures in $C2/m-B_6$, $C2/m-B_8$ and $C2/m-B_{12}$. As for the band structures and PDOS of the predicted boron clathrates at ambient pressure plotted in Fig. S11 [39], $C2/m-B_6$ is a semi-conductor with a indirect band gap of about 0.88 eV. In $C2/m-B_6$, the B-s electrons have competitive contribution with B-p electrons in the valence bands around the Fermi energy, implying the visible hybridization between B-s and B-p in $C2/m-B_6$, while $C2/m-B_8$ and $C2/m-B_{12}$ are typical metals and the B-p electrons play predominant role around the Fermi energy. Moreover, the calculations of COHP in Fig. S12 [39] illustrate that the B-B exhibits bonding characteristics below the Fermi energy in all the three predicted boron clathrates and their ICOHP strengths are comparable with boron allotropes such as $o-B_{16}$ [29].

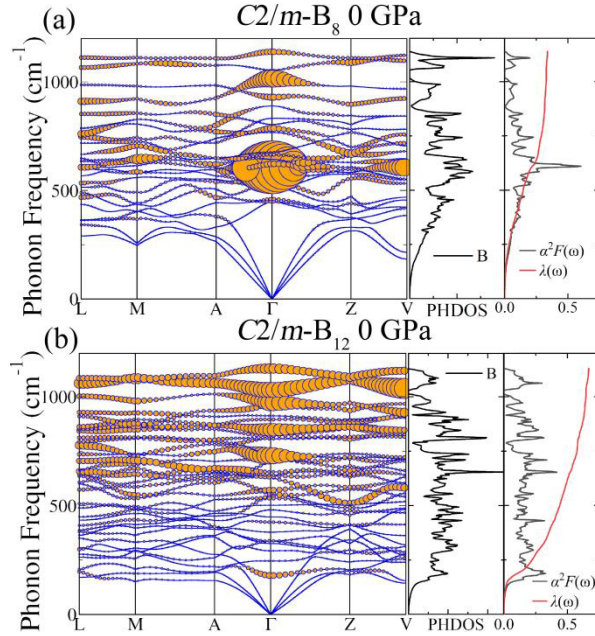


FIG. 5. The calculated phonon curves, PHDOS, Eliashberg spectral function $\alpha^2F(\omega)$, the electron-phonon integral $\lambda(\omega)$ for $C2/m-B_8$ and $C2/m-B_{12}$ at ambient pressure, respectively. The orange solid dots represents the EPC constant λ and the radii are proportional to the strength.

Considering the metallicity of $C2/m-B_8$ and $C2/m-B_{12}$ at ambient pressure, we carried out the EPC calculations to study their superconducting properties. The calculated EPC constants, projected phonon density of states (PHDOS), Eliashberg spectral function $\alpha^2F(\omega)$ and the electron-phonon integral $\lambda(\omega)$ for $C2/m-B_8$ and $C2/m-B_{12}$ are shown in Fig. 5, and the radii of the orange dots denote the EPC strength of the vibration modes. In the aspect of vibration modes, frequencies larger than 300 cm⁻¹ are more decorated with the solid dots, which correlates with more than 70% of the integral $\lambda(\omega)$ in $C2/m-B_8$ [Fig. 5 (a)], and the large distribution of the

phonon modes around 500-600 cm^{-1} , such as at Γ point, result in a sudden enhancement about 29% of the integral $\lambda(\omega)$ [Fig. 5 (a)]. In EPC calculations of $C2/m\text{-B}_{12}$ [Fig. 5 (b)], we can observe EPC strength distribution around 220 cm^{-1} at Γ point, which relates to a peak in $\alpha^2F(\omega)$, and about 29% of the integral $\lambda(\omega)$ is from the vibration modes below 220 cm^{-1} , indicating the impact of the relatively low frequencies to the EPC constant. The calculated EPC constant λ is 0.34 for $C2/m\text{-B}_8$ at ambient pressure with a estimated T_c value of 0.96 K ($\mu^*=0.1$), suggesting weak superconductivity. Nevertheless, the EPC constant λ is 0.66 for $C2/m\text{-B}_{12}$ at ambient pressure and the estimated T_c value is 16.12 K ($\mu^*=0.1$). This is comparable to the superconducting boron allotropes like $c\text{-B}_{24}$ (13.8 K) [67], $I4/mmm\text{-B}_4$ (19.8 K), $Pm\text{-B}_{17}$ (15.4 K) [27] and $o\text{-B}_{16}$ (14.2 K) [29] at ambient pressure.

TABLE. 3. The bulk modulus B (GPa), shear modulus G (GPa), Young's modulus E (GPa) and the Vickers hardness (H_v) estimated by different formulas [49-51] of the predicted boron clathrates.

	B (GPa)	G (GPa)	E (GPa)	σ	H_v^{Chen} (GPa)	H_v^{Tian} (GPa)	H_v^{Mazhni} (GPa)
$C2/m\text{-B}_6$	252.36	267.84	593.54	0.11	53.44	51.53	49.39
$C2/m\text{-B}_8$	188.15	118.66	294.15	0.24	16.07	16.02	13.53
$C2/m\text{-B}_{12}$	151.48	58.923	156.48	0.33	4.19	5.64	8.55

Subsequently, we calculated the mechanical properties of the predicted clathrates $C2/m\text{-B}_6$, $C2/m\text{-B}_8$ and $C2/m\text{-B}_{12}$ at ambient pressure, and they satisfy the mechanical stability on the basis of Born stability criteria [63]. As listed in Table. 3, the hardness values of $C2/m\text{-B}_8$ and $C2/m\text{-B}_{12}$ are below 20 GPa, while the value of $C2/m\text{-B}_6$ reaches around 49-53 GPa using different formula [52-54], which reaches the threshold of super-hardness [14, 15] and is comparable to the super-hard borides such as ReB_2 (48 GPa), CrB_4 (48 GPa), $\alpha\text{-BeB}_6$ (46 GPa), WB_5 (45 GPa) and WB_4 (43.3 GPa) [16, 17, 20, 21]. Moreover, we investigated the stress-strain relationships of the super-hard $C2/m\text{-B}_6$ under various loading conditions. As depicted in Fig. 6 (a), the tensile strain calculations are along the [001], [100], [010], [101], [110], [001] and [111] directions. The ideal tensile strength is about 28 GPa, owing to the (110) plane is the easy cleavage plane, and the tensile strength along the other directions are larger than 30 GPa. Following the tensile strain calculations [Fig. 6(a)], we studied the shear stress by loading the strain on the easy cleavage plane (110) in Fig. 6 (b). The shear directions along $[1\bar{1}0]$ and $[1\bar{1}\bar{1}]$ have isotropic respond to the shear strain within the $\varepsilon=0.1$. Different from the other two shear directions, there is a sharp decrease under

the deformation of $\varepsilon=0.15$, suggesting the weakest shear stress or the ideal shear strength of 23 GPa along the [001] direction of (110) plane.

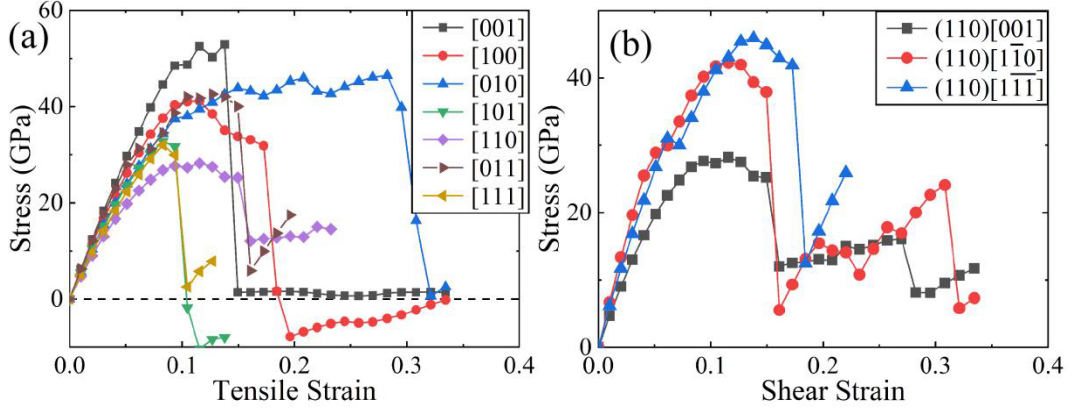


FIG. 6. Stress-strain relations of $C2/m-B_6$ under (a) tensile and (b) shear deformations.

To further validate the thermodynamic stability of $C2/m-B_6$ and $C2/m-B_{12}$, we performed the AIMD (NVT ensemble) simulations under ambient pressure at 300 K and 500 K. The simulation results along with the intermediate structures in Fig. S13 (a) and (b) [39] illustrate that $C2/m-B_6$ and $C2/m-B_{12}$ could withstand their stability under ambient condition without obvious structural destruction, suggesting that $C2/m-B_6$ and $C2/m-B_{12}$ have the potential to be synthesized under appropriate experimental condition. In addition, we further carried out the AIMD (NVT ensemble) simulations for the precursors of UB_3-C2/m and $UB_{12}-C2/m$ at 500 K under their lowest dynamical stable pressure. As shown in Fig. S13(c) [39], the precursor structures could preserve their stability at 500 K as well. Moreover, the compounds and boron structures were rechecked by AIMD (NPT ensemble) at 300 K in Fig. S14 [39], which further suggests the dynamical stability at finite temperature. As for the precursors, the $UB_{12}-Fm-3m$ is one of the experimentally reported structure and the predicted $UB_{12}-C2/m$ has lower enthalpy after 167 GPa. Their enthalpy difference is less than 0.1 eV/atom after 120 GPa [Fig. S1] [39]. Hence we propose that $UB_{12}-C2/m$ has potential for synthesizing under high pressure and high temperature (HPHT) combining DAC and laser heating around 120 GPa, or we can expect the structure transformation under higher pressure and then release the pressure. In UB_3-C2/m , we propose to take the experimental $Imm2-Na_2B_{29}$ as reference [68]. The $Imm2-Na_2B_{29}$ has positive formation energy of 3.03 meV/atom comparing with Na plus B, which is far from the convex hull [68]. It could be synthesized using sodium and boron, which are filled into a pre-boronated tantalum tube and exposed to reaction conditions (1050 °C, 3 h, plus 1150 °C, 3 h). Then an excess of sodium is removed by distillation at 10^{-2} mbar and 350 °C [69]. Furthermore, Ref. 70 points out that uranium borides could be

synthesized combining UO_2 , boron carbide (B_4C), graphite and the partial pressures of CO. Thus, we assume that $\text{UB}_3\text{-C2}/m$ is likely to be synthesized when considering the above mentioned experimental clues.

Overall, our calculations provide theoretical evidence to support the existence of the predicted super-hard $\text{C2}/m\text{-B}_6$ and superconducting $\text{C2}/m\text{-B}_{12}$ under certain experimental conditions. The removing of U atoms in the precursors may be one of the access for achieving the predicted boron clathrates, we can also expect the emerging of $\text{C2}/m\text{-B}_6$ and $\text{C2}/m\text{-B}_{12}$ when the experiments meet appropriate requirements during the synthesizing of boron allotopes.

IV. Conclusion

In summary, using the first-principles calculations and crystal structure prediction methods in MAGUS, we systematically investigated the phase diagram of U-B compounds within 200 GPa. We have proposed 8 unique compounds that are possible to be synthesized and 4 exotic stoichiometries. These predicted compounds have either net or caged structure units which are potential precursors of the boron allotropes. After removing the uranium atoms, we studied the stability, electronic structures, superconductivity and mechanical properties of the corresponding boron structures. We predicted three boron clathrates under ambient pressure, among which $\text{C2}/m\text{-B}_6$ is a super-hard material with the estimated Vickers hardness value about 49-53 GPa, while $\text{C2}/m\text{-B}_{12}$ is superconducting with the T_c value of 16.12 K. $\text{C2}/m\text{-B}_6$ and $\text{C2}/m\text{-B}_{12}$ have potential for synthesizing at ambient condition and they are potential materials for future applications. Our exploration enriches the phase diagram of U-B compounds and boron, which is helpful for designing unique and safer material for the nuclear industry and provides insights for studies on the unique boron based materials.

Acknowledgement

This work was supported by the National Natural Science Foundation of China (Grant Nos. 12474018, 52272265, 12204138 12125404 and 123B2049), the National Key R&D Program of China (Grant Nos. 2023YFA1607400 and 2022YFA1403201), the Basic Research Program of Jiangsu (Grant BK20233001, BK20241253), the Jiangsu Funding Program for Excellent Postdoctoral Talent (Grants 2024ZB002 and 2024ZB075), the Postdoctoral Fellowship Program of CPSF (Grant GZC20240695), the AI & AI for Science program of Nanjing University, and the Fundamental Research Funds for the Central Universities. The calculations were supported by HPC

platform of ShanghaiTech University, supercomputers at the High-Performance Computing Center of Collaborative Innovation Center of Advanced Microstructures, the high-performance supercomputing center of Nanjing University.

References

- [1] T. Ogitsu, E. Schwegler and G. Galli, β -Rhombohedral Boron: At the Crossroads of the Chemistry of Boron and the Physics of Frustration, *Chem. Rev.* 113, 3425-3449 (2013).
- [2] G. Parakhonskiy, N. Dubrovinskaia, E. Bykova, R. Wirth and L. Dubrovinsky, Experimental pressure-temperature phase diagram of boron resolving the long-standing enigma, *Sci. Rep.* 1, 96 (2011).
- [3] B. Albert and H. Hillebrecht, Boron: Elementary Challenge for Experimenters and Theoreticians, *Angew. Chem. Int. Ed.* 48, 8640-8668 (2009).
- [4] A. G. Van Der Geest and A. N. Kolmogorov, Stability of 41 metal-boron systems at 0 GPa and 30 GPa from first principles *Calphad* 46, 184 (2014).
- [5] J. Kortus, I. I. Mazin, K. D. Belashchenko, V. P. Antropov, and L. L. Boyer, Superconductivity of Metallic Boron in MgB₂, *Phys. Rev. Lett.* 86, 4656 (2001).
- [6] J. Nagamatsu, N. Nakagawa, T. Muranaka, Y. Zenitani, and J. Akimitsu, Superconductivity at 39 K in magnesium diboride *Nature* 410, 63 (2001).
- [7] C. Y. Pei, J. F. Zhang, Q. Wang, Y. Zhao, L. L. Gao, C. S. Gong, S. J. Tian, R. T. Luo, M. T. Li, W. G. Yang, Z. Y. Lu, H. C. Lei, K. Liu, and Y. P. Qi, Pressure-induced superconductivity at 32 K in MoB₂, *Nat. Sci. Rev.* 10, nwad034 (2023).
- [8] X. H. Liu, X. W. Huang, P. Song, C. Z. Wang, L. Y. Zhang, P. Lv, L. L. Liu, W. F. Zhang, J. H. Cho, and Y. Jia, Strong electron-phonon coupling superconductivity in compressed α -MoB₂ induced by double Van Hove singularities, *Phys. Rev. B* 106, 064507 (2022).
- [9] J. Lim, A. C. Hire, Y. Quan, J. S. Kim, S. R. Xie, S. Sinha, R. S. Kumar, D. Popov, C. Park, R. J. Hemley, Y. K. Vohra, J. J. Hamlin, R. G. Hennig, P. J. Hirschfeld and G. R. Stewart, Creating superconductivity in WB₂ through pressure-induced metastable planar defects, *Nat. Commun.* 13, 7901 (2022).
- [10] C. Y. Pei, J. F. Zhang, C. S. Gong, Q. Wang, L. L. Gao, Y. Zhao, S. J. Tian, W. Z. Cao, C. H. Li, Z. Y. Lu, H. C. Lei, K. Liu and Y. P. Qi, Distinct superconducting behaviors of pressurized WB₂ and ReB₂ with different local B layers, *Sci. China Phys. Mech. Astron.* 65, 287412 (2022).
- [11] H. J. Choi, S. G. Louie, and M. L. Cohen, Prediction of superconducting properties of CaB₂ using anisotropic Eliashberg theory, *Phys. Rev. B* 80, 064503 (2009).
- [12] J. Wang, X. Song, X. Shao, B. Gao, Q. Li, and Y. Ma, High-Pressure Evolution of Unexpected Chemical Bonding and Promising Superconducting Properties of YB₆, *J. Phys. Chem. C* 122, 27820 (2018).
- [13] Y. Liang, M. Xu, S. Lin, X. Yuan, Z. Qu, J. Hao, and Y. Li, Pressure-induced boron clathrates with ambient-pressure superconductivity, *J. Mater. Chem. C* 9, 13782 (2021).
- [14] Z. Zhang and J. Brgoch, Treating Superhard Materials as Anomalies, *J. Am.*

Chem. Soc. 144, 18075 (2022).

- [15] R. B. Kaner, J. J. Gilman, and S. H. Tolbert, Designing Superhard Materials, Science 308, 1268 (2005).
- [16] H.-Y. Chung, M. B. Weinberger, J. B. Levine, A. Kavner, J.-M. Yang, S. H. Tolbert, and R. B. Kaner, Synthesis of ultra-incompressible superhard rhenium diboride at ambient pressure, Science 316, 436 (2007).
- [17] R. Mohammadi, A. T. Lech, M. Xie, B. E. Weaver, M. T. Yeung, S. H. Tolbert, and R. B. Kaner, Tungsten tetraboride, an inexpensive superhard material, Proc. Natl. Acad. Sci. U. S. A. 108, 10958 (2011).
- [18] H. Gou, N. Dubrovinskaia, E. Bykova, A. A. Tsirlin, D. Kasinathan, W. Schnelle, A. Richter, M. Merlini, M. Hanfland, A. M. Abakumov, D. Batuk, G. Van Tendeloo, Y. Nakajima, A. N. Kolmogorov, and L. Dubrovinsky, Discovery of a Superhard Iron Tetraboride Superconductor, Phys. Rev. Lett. 111, 157002 (2013).
- [19] T. Ma, H. Li, X. Zheng, S. Wang, X. Wang, H. Zhao, S. Han, J. Liu, R. Zhang, P. Zhu, Y. Long, J. Cheng, Y. Ma, Y. Zhao, C. Jin, and X. Yu, Ultrastrong Boron Frameworks in ZrB₁₂: A Highway for Electron Conducting, Adv. Mater. 29, 1604003 (2017).
- [20] H. Niu, J. Wang, X. Q. Chen, D. Li, Y. Li, P. Lazar, R. Podlucky, and A. N. Kolmogorov, Structure, bonding, and possible superhardness of CrB₄, Phys. Rev. B 85, 144116 (2012).
- [21] A. G. Kvashnin, H. A. Zakaryan, C. Zhao, Y. Duan, Y. A. Kvashnina, C. Xie, H. Dong, and A. R. Oganov, New Tungsten Borides, Their Stability and Outstanding Mechanical Properties, J. Phys. Chem. Lett. 9, 3470 (2018).
- [22] K. Zhao, Q. Wang, W. Li, Q. Yang, H. Yu, F. Han, H. Liu, and S. Zhang, Orthorhombic ScB₃ and hexagonal ScB₆ with high hardness, Phys. Rev. B 105, 094104 (2022).
- [23] L. Wu, B. Wan, H. Liu, H. Gou, Y. Yao, Z. Li, J. Zhang, F. Gao, and H. k. Mao, Coexistence of Superconductivity and Superhardness in Beryllium Hexaboride Driven by Inherent Multicenter Bonding, J. Phys. Chem. Lett. 7, 4898 (2016).
- [24] S. Han, L. Yu, Y. Liu, B. Zhao, C. Wang, X. Chen, Y. Zhang, R. Yu, and X. Liu, Clathrate-Like Alkali and Alkaline-Earth Metal Borides: A New Family of Superconductors with Superior Hardness, Adv. Funct. Mater. 33, 2213377 (2023).
- [25] Q. Wang, H. Li, J. Wei, T. Zhong, L. Zhu, X. Zhang, H. Liu, and S. Zhang, Hardness and superconductivity in tetragonal LiB₄ and NaB₄, J. Chem. Phys. 159, 234707 (2023).
- [26] Y. Ma, J. Dong, H. Chen, H. Jiang, X. Jiang, J. Wang, D. Duan, and J. Sun, Ambient-pressure hardness and superconductivity in sp^2 and sp^3 bonded Ce-B compounds, Phys. Rev. B 110, 134515 (2024).
- [27] S. Zhang, X. Du, J. Lin, A. Bergara, X. Chen, X. Liu, X. Zhang and G. Yang, Superconducting boron allotropes, Phys. Rev. B 101, 174507 (2020).
- [28] Y. Liang, M. Xu, Z. Qu, S. Lin, J. Hao, and Y. Li, A cage boron allotrope with high superconductivity at ambient pressure, J. Mater. Chem. C 9, 8258 (2021).
- [29] Z. Cui, Q. Yang, X. Qu, X. Zhang, Y. Liu and G. Yang, A superconducting boron allotrope featuring anticlinal pentapyramids, J. Mater. Chem. C 10, 672 (2022).

- [30] I. A. Kruglov, A. G. Kvashnin, A. F. Goncharov, A. R. Oganov, S. S. Lobanov, N. Holtgrewe, S. Jiang, V. B. Prakapenka, E. Greenberg, and A. V. Yanilkin, Uranium polyhydrides at moderate pressures: Prediction, synthesis, and expected superconductivity, *Sci. Adv.* 4, eaat9776 (2018).
- [31] X. Wang, M. Li, F. Zheng, and P. Zhang, Crystal structure prediction of uranium hydrides at high pressure: A new hydrogen-rich phase, *Phys. Lett. A* 382, 2959-2964 (2018).
- [32] M. Liu, Y. Shi, M. Liu, D. Li, W. Mo, T. Fa, B. Bai, X. Wang, and X. Chen, First-principles comprehensive study of electronic and mechanical properties of novel uranium hydrides at different pressures, *Prog. Nat. Sci.: Mater. Int.* 30, 251-259 (2020).
- [33] J. Wu, Y.-C. Wang, Y. Liu, B. Sun, Y. Zhao, J. Xian, X. Gao, H. Liu and H. Song, First-principles study on the electronic structure transition of β -UH₃ under high pressure, *Matter Radiat. Extremes* 7, 058402 (2022).
- [34] J. Wu, B. Zhu, C. Ding, C. Pei, Q. Wang, J. Sun, and Y. Qi, Superconducting ternary hydrides in Ca-U-H under high pressure, *J. Phys.: Condens. Matter* 36, 165703 (2024).
- [35] J.-P. Dancausse, E. Gering, S. Heathman and U. Benedict, Compression study of uranium borides UB₂, UB₄ and UB₁₂ by synchrotron X-ray diffraction, *J. Alloys Compd.* 189, 205-208 (1992).
- [36] E. Jossou, L. Malakkal, B. Szpunar, D. Oladimeji, and J. A. Szpunar, A first principles study of the electronic structure, elastic and thermal properties of UB₂, *J. Nucl. Mater.* 490, 41-48 (2017).
- [37] G. Kresse, and J. Furthmüller, Efficient iterative schemes for ab initio total-energy calculations using a plane-wave basis set, *Phys. Rev. B* 54, 11169 (1996).
- [38] H. J. Monkhorst, and J. D. Pack, Special points for Brillouin-zone integrations, *Phys. Rev. B* 13, 5188 (1976).
- [39] See Supplementary materials at [URL] for detailed calculation parameters, lattice parameters of the predicted structures, relative enthalpy of U-B compounds under high pressure, calculated phonon spectra, convex hull including ZPE, electronic structures, ELF results, COHP results, AIMD simulation results, which includes Refs. [40-42].
- [40] [first reference in Supplemental Material not already in paper] V.I. Anisimov, J. Zaanen, and O.K. Andersen, Band theory and Mott insulators - Hubbard-U instead of Stoner-I, *Phys. Rev. B* 44, 943 (1991).
- [41] [second reference in Supplemental Material not already in paper] S. L. Dudarev, G. A. Botton, S. Y. Savrasov, C. J. Humphreys, and A. P. Sutton, Electron-energy-loss spectra and the structural stability of nickel oxide: An LSDA+U study, *Phys. Rev. B* 57, 1505 (1998).
- [42] [last reference in Supplemental Material not already in paper] P. B. Allen and R. C. Dynes, Transition temperature of strong-coupled superconductors reanalyzed, *Phys. Rev. B* 12, 905 (1975).
- [43] J. Wang, H. Gao, Y. Han, C. Ding, S. Pan, Y. Wang, Q. Jia, H.-T. Wang, D. Xing, and J. Sun, MAGUS: machine learning and graph theory assisted universal structure

searcher, Natl. Sci. Rev. 10, nwad128, (2023).

[44] K. Xia, H. Gao, C. Liu, J. Yuan, J. Sun, H. T. Wang, and D. Xing, A novel superhard tungsten nitride predicted by machine learning accelerated crystal structure search, Sci. Bull. 63, 817 (2018).

[45] J. P. Perdew, K. Burke, and M. Ernzerhof, Generalized Gradient Approximation Made Simple, Phys. Rev. Lett. 77, 3865 (1996).

[46] P. E. Blöchl, Projector augmented-wave method, Phys. Rev. B 50, 17953 (1994).

[47] P. C. Müller, C. Ertural, J. Hempelmann, and R. Dronskowski, Crystal Orbital Bond Index: Covalent Bond Orders in Solids J. Phys. Chem. C 125, 7959-7970 (2021).

[48] A. Togo and I. Tanaka, First principles phonon calculations in materials science, Scr. Mater. 108, 1 (2015).

[49] G. J. Martyna, M. L. Klein, and M. Tuckerman, Nosé-Hoover chains: The canonical ensemble via continuous dynamics, J. Chem. Phys. 97, 2635 (1992).

[50] Y. Le Page and P. Saxe, Symmetry-general least-squares extraction of elastic data for strained materials from *ab initio* calculations of stress, Phys. Rev. B 65, 104104 (2002).

[51] R. Hill, The Elastic Behaviour of a Crystalline Aggregate, Proc. Phys. Soc., Sect. A 65, 349 (1952).

[52] X. Q. Chen, H. Niu, D. Li, and Y. Li, Modeling hardness of polycrystalline materials and bulk metallic glasses, Intermetallics 19, 1275 (2011).

[53] Y. Tian, B. Xu, and Z. Zhao, Microscopic theory of hardness and design of novel superhard crystals, Int. J. Refract. Met. Hard Mater. 33, 93 (2012).

[54] E. Mazhnik and A.R. Oganov, A model of hardness and fracture toughness of solids, J. Appl. Phys. 126, 125109 (2019).

[55] P. Giannozzi, S. Baroni, N. Bonini, M. Calandra, R. Car, C. Cavazzoni, D. Ceresoli, G. L. Chiarotti, M. Cococcioni, I. Dabo, A. D. Corso, S. de Gironcoli, S. Fabris, G. Fratesi, R. Gebauer, U. Gerstmann, C. Gougoussis, A. Kokalj, M. Lazzeri, L. Martin-Samos, N. Marzari, F. Mauri, R. Mazzarello, S. Paolini, A. Pasquarello, L. Paulatto, C. Sbraccia, S. Scandolo, G. Sclauzero, A. P Seitsonen, A. Smogunov, P. Umari and R. M Wentzcovitch, QUANTUM ESPRESSO: a modular and opensource software project for quantum simulations of materials, J. Phys.: Condens. Matter 21, 395502 (2009).

[56] C.-S. Yoo, H. Cynn and P. Soderlind, Phase diagram of uranium at high pressures and temperatures, Phys. Rev. B 57, 10359 (1998).

[57] A. Oganov, J. Chen, C. Gatti, Y. Ma, Y. Ma, C. Glass, Z. Liu, T. Yu, O. Kurakevych, and V. Solozhenko, Ionic high-pressure form of elemental boron, Nature (London) 457, 863 (2009)

[58] K. P. Hilleke, T. Ogitsu, S. Zhang, and E. Zurek, Structural motifs and bonding in two families of boron structures predicted at megabar pressures, Phys. Rev. Mater. 5, 053605 (2021).

[59] H. Xiao, Y. Dan, B. Suo, and X. Chen, Comment on “Accelerated discovery of new 8-electron half-Heusler compounds as promising energy and topological quantum materials, J. Phys. Chem. C 124, 2247 (2020).

- [60] W. Sun, C. J. Bartel, E. Arca, S. R. Bauers, B. Matthews, B. Orvananos, B.-R. Chen, M. F. Toney, L. T. Schelhas, W. Tumas, J. Tate, A. Zakutayev, S. Lany, A. M. Holder, and G. Ceder, A map of the inorganic ternary metal nitrides, *Nat. Mater.* 18, 732 (2019).
- [61] F. W. Glaser, D. Moskowitz and B. Post, A Study of Some Binary Hafnium Compounds, *JOM* 5, 1119-1120 (1953).
- [62] I. S. Flyagina, A. A. Markov, A. I. Malkin, D. A. Popov, V. N. Chuvildeev, Metastable aluminum boride: density functional theory study of prerequisites of formation, *Int. J. Quantum Chem.* 123:e27219 (2023).
- [63] F. Mouhat and F. X. Coudert, Necessary and sufficient elastic stability conditions in various crystal systems, *Phys. Rev. B* 90, 224104 (2014).
- [64] B. Zhao, X. Wang, L. Yu, Y. Liu, X. Chen, B. Yang, G. Yang, S. Zhang, L. Gu, and X. Liu, Fabrication of Alkali Metal Boride: Honeycomb-Like Structured NaB₄ with High Hardness and Excellent Electrical Conductivity, *Adv. Funct. Mater.* 32, 2110872 (2022).
- [65] G. Parakhonskiy, N. Dubrovinskaia, E. Bykova, R. Wirth and L. Dubrovinsky, High pressure synthesis and investigation of single crystals of metastable boron phases, *High Press. Res.* 33, 673 (2013).
- [66] D. Y. Kim, S. Stefanoski, O. O. Kurakevych and T. A. Strobel, Synthesis of an open-framework allotrope of silicon, *Nat. Mater.* 14, 169-173 (2015).
- [67] Q. Yang, J. Lv, Q. Tong, X. Du, Y. Wang, S. Zhang, G. Yang, A. Bergara and Y. Ma, Hard and superconducting cubic boron phase via swarm-intelligence structural prediction driven by a machine-learning potential, *Phys. Rev. B* 103, 024505 (2021).
- [68] X.-L. He, X. Dong, Q. S. Wu, Z. Zhao, Q. Zhu, A. R. Oganov, Y. Tian, D. Yu, X.-F. Zhou, and H.-T. Wang, Predicting the ground-state structure of sodium boride, *Phys. Rev. B* 97, 100102(R) (2018).
- [69] B. Albert, K. Hofmann, C. Fild, H. Eckert, M. Schleifer, and R. Grurhn, “NaB₁₅”: A New Structural Description Based on X-ray and Neutron Diffraction, Electron Microscopy, and Solid-State NMR Spectroscopy, *Chem. Eur. J.* 6, 2531 (2000).
- [70] J. Turner, F. Martini, J. Buckley, G. Phillips, S.C. Middleburgh and T.J. Abram, Synthesis of candidate advanced technology fuel: Uranium diboride (UB₂) via carbo/borothermic reduction of UO₂, *J. Nucl. Mater.*